Strain induced ionic conductivity enhancement in epitaxial Ce0.9Gd0.1O22d

Kant, K. Mohan; Esposito, Vincenzo; Pryds, Nini

Published in:
Applied Physics Letters

Link to article, DOI:
10.1063/1.3676659

Publication date:
2012

Document Version
Publisher's PDF, also known as Version of record

AIP | Applied Physics Letters

Strain induced ionic conductivity enhancement in epitaxial Ce0.9Gd0.1O2−δ thin films

K. Mohan Kant, V. Esposito, and N. Pryds

Citation: Appl. Phys. Lett. **100**, 033105 (2012); doi: 10.1063/1.3676659
View online: http://dx.doi.org/10.1063/1.3676659
View Table of Contents: http://apl.aip.org/resource/1/APPLAB/v100/i3
Published by the American Institute of Physics.

Strain induced ionic conductivity enhancement in epitaxial $Ce_{0.9}Gd_{0.1}O_{2-\delta}$ thin films

K. Mohan Kant,[a] V. Esposito, and N. Pryds[b]
Fuel Cells and Solid State Chemistry Division, Risø Denmark Technical University, Roskilde 4000, Denmark

(Received 25 April 2011; accepted 17 December 2011; published online 17 January 2012)

Strained epitaxial $Ce_{0.9}Gd_{0.1}O_{2-\delta}$ (CGO) thin films are deposited on MgO(001) substrates with $SrTiO_3$ (STO) buffer layers. The strain in CGO epitaxial thin films is induced and controlled by varying the thickness of STO buffer layers. The induced strain is found to significantly enhance the *in-plane* ionic conductivity in CGO epitaxial thin films. The ionic conductivity is found to increase with decrease in buffer layer thickness. The tailored ionic conductivity enhancement is explained in terms of close relationships among epitaxy, strain, and ionic conductivity. © *2012 American Institute of Physics*. [doi:10.1063/1.3676659]

Fabrication of devices based on electrochemical reactions such as solid oxide fuel cells (SOFC) depends greatly on the development of solid oxide electrolyte materials with enhanced ionic conductivity at lower and intermediate operating temperatures. $Ce_{0.9}Gd_{0.1}O_{2-\delta}$ (CGO) is one such solid oxide electrolyte material that has a great potential; it can even be a replacement to the commonly used yttrium stabilized zirconia (YSZ) in SOFC.[1,2] Owing to the paramount importance of CGO, especially in thin film form, it has been thoroughly investigated.[3–5] It is now possible to deposit polycrystalline as well as highly textured CGO thin films on to various substrates like MgO(001), $LaAlO_3$(001), $NdGaO_3$(001), sapphire, and Si(001).[6–12] Epitaxial CGO thin films can also be deposited by properly choosing the substrate and experimental conditions. With regards to the improvement of ionic conductivity in solid oxide electrolyte materials (ionic conductors in general), it is understood that strain in the material also plays an imperative role.[13] For example, it has been reported that ionic conductivity in multi-layered YSZ epitaxial thin film system increases when the fluorite lattice is strained. In another report, it has been shown that lattice-strain induced in polycrystalline ceria by doping it with trivalent cations (Nd^{3+} and Nd^{+3}/Sm^{3+}as compared to Gd^{+3}) not only enhances the ionic conductivity but also changes the activation energy.[14–17] However, the information available on epitaxy and its influence on the electrical properties of CGO thin films is limited. The major difficulty in evaluating and explaining the electrical properties of CGO thin films is to separate the ionic conductivity from the total measured conductivity. In this work, the influence of substrate/buffer layer induced strain on the overall electrical transport in epitaxial CGO thin films will be elucidated.

Epitaxial CGO_{250nm} thin films (thickness: 250 nm) are deposited on MgO(001) and buffered MgO(001)/STO substrates. STO buffer layer thicknesses used are 10 (MgO(001)/STO_{10nm}), 20 (MgO(001)/STO_{20nm}), and 50 nm (MgO(001)/STO_{50nm}). The reason to use the above mentioned substrates is to benefit from the characteristics of MgO(001) and STO(001). MgO(001) is an insulator ($R \sim 10^9\ \Omega$ at 800 °C) even at high temperatures and therefore, its contribution to the total measured conductivity is negligible.[18] However, MgO(001) ($a = b = c = 4.219$ Å) is incompatible for the epitaxial growth of CGO ($a = b = c = 5.418$ Å) thin films due to its large lattice mismatch $\left(|a_{CGO} - a_{MgO(110)}|/a_{CGO} \times 100 = 9.1\%\right)$ resulting in blocking effects due to large grain boundary network.[13,19] For CGO films deposited on MgO(001), occurrence of dislocations starts soon after film nucleation to accommodate the large mismatch with typically large mosaic spread accompanied by columnar growth.[9,20] The critical thickness at which dislocations begin to form varies (approximately) inversely with lattice mismatch.[21] On the other hand, lower mismatched substrate such as STO(001) ($a = b = c = 3.907$ Å), $\left(|a_{CGO} - a_{STO(110)}|/a_{STO(110)} \times 100 = 1.9\%\right)$ is compatible for the epitaxial growth of CGO thin films; and STO exhibits electronic conductivity above 300 °C under only reducing conditions, low oxygen partial pressures (P_{O_2}) $< 10^{-17}$ atm and insulating behaviour at $P_{O_2} > 10^{-15}$ atm.[22] Additionally, preliminary transport measurements in the temperature range 400–900 °C on MgO(001) and MgO(001)/$STO_{10/20/50nm}$ substrates indicated that their contribution to the total conductivity is negligible. Moreover, in this work, the conductivity of epitaxial CGO films are measured in air (high P_{O_2}) where the ionic conductivity has been demonstrated to be dominant.[9,19]

Pulsed laser deposition (PLD) technique was used to deposit the thin films in this work. X-ray diffraction (XRD) technique was used not only to understand the epitaxial nature of CGO thin films but also to measure the strain in them. The electrical transport properties are studied in air using AC impedance and two probe DC techniques in the temperature range 400–900 °C [see supplementary material for experimental details[25]].

XRD patterns [see Figure S1 in supplementary material[25]] of MgO(001)/$STO_{10/20/50nm}$ and MgO(001)/$STO_{10/20/50\ nm}$/CGO_{250nm} thin films reveal the cubic fluorite structure of CGO with no evidence of secondary phases. Only (00*l*) reflections of MgO, STO, and CGO appear in the diffraction pattern indicating that STO and CGO films have *c*-axis normal to substrate surface. The *out-of-plane* lattice constant of

[a]Present address: Spintronics and Thin film Magnetism Laboratory, Department of Physics, Indian Institute of Science, Bangalore, India.
[b]Author to whom correspondence should be addressed. Electronic mail: nipr@risoe.dtu.dk.

$STO_{10/20/50nm}$ and CGO_{250nm} films is found to be compressed, as expected due to boundary conditions imparted by MgO(001) and MgO(001)/$STO_{10/20/50nm}$ substrates. When the *a-b* plane of the $STO_{10/20/50nm}$ and CGO_{250nm} films expand coherently with respect to MgO(001) and MgO(001)/$STO_{10/20/50nm}$, their *c*-axis gets compressed substantially lower than the bulk value leading to compressive strain as shown by the measured *c*-axis lattice constants and strain in Figures 1(c) and 1(d). The relative strain (ε) is estimated from the relation: $s = (\alpha - \alpha_{bulk})/\alpha_{bulk}$, where α_{bulk} is the lattice constant of unstrained polycrystalline CGO_{250nm} (a = b = c = 5.418 Å) and STO (a = b = c = 3.907 Å) thin films. STO_{10nm} film exhibited larger strain of 1.0% among the buffer layers. The *in-plane* lattice parameters were determined by (*h00*) reflections scanned under a glancing incidence x-ray diffraction condition. The *in-plane* lattice parameters found to be 5.460 ± 0.002 Å, 5.449 ± 0.002 Å, and 5.427 ± 0.002 Å for CGO_{250nm} deposited on MgO/$STO_{10/20/50\,nm}$. The *in-plane* lattice strain found to be 0.8%, 0.6%, and 0.2%, respectively, for MgO/$STO_{10/20/50nm}$/CGO_{250nm} thin films. The *out-of-plane* lattice parameter (c_{CGO}) was found to be 5.308 ± 0.002 Å, 5.332 ± 0.002 Å, 5.376 ± 0.002 Å for MgO(001), $STO_{10/20/50\,nm}$, and CGO_{250nm}, respectively. CGO_{250nm} films deposited on STO 10, 20, and 50 nm buffer layers resulted in 1.9%, 1.5%, and 0.7% strain, respectively, in CGO lattice (Figure 1(d)). This clearly demonstrates that STO buffer layer improves lattice matching between MgO(001) and CGO by inducing strain. No strain is measured in polycrystalline CGO_{250nm} films deposited directly onto MgO(001) under the same deposition conditions. A rocking curve measurement on the CGO(002) reflection supports these observations and showed that full width at half maximum (FWHM) was in the range of 0.21° to 0.22° for the films grown on MgO(001)/$STO_{10/20/50nm}$ (Figure S1(d), supplementary material[25]). However, FWHM of MgO(001)/CGO_{250nm} films without STO buffer layer is observed to be 3.49° which is one order magnitude larger than that observed in CGO films grown on MgO(001)/$STO_{10/20/50nm}$ (Figure S1(c), supplementary material[25]). The observed shift in peak position is probably a consequence of the strain effect in CGO films due to high degree of their epitaxy on STO buffer layers. Mosaic and columnar growth is observed in MgO(001)/CGO_{250nm} and MgO(001)/Sm doped CeO_2 films due to large misfit between substrate and thin film.[9] However, low lattice misfit between MgO(001)/$STO_{10/20/50nm}$ and CGO_{250nm} in the present study resulted in lower strain and epitaxy in CGO_{250nm} films.

In order to exactly determine the epitaxial nature of STO buffer layers and CGO_{250nm} films on STO buffer layers, phi (Φ) scan of x-ray diffraction was carried out. The Φ scan on (301) peak of STO in MgO(001)/STO_{50nm} film shows three distinct peaks with same intensity and nearly 90° spacing between the peaks (Figure 1(a)). Similar trend was observed for CGO(311) reflection, with a displacement of 45° with respect to MgO(311) (Figure 1(b)). The FWHM values for the CGO peaks are in the range 0.23°–0.25°, which are consistent with previous rocking curve measurements. These results indicate that epitaxial growth of CGO(001) on MgO(001) with $STO_{10/20/50nm}$ buffer layer has been achieved through the rotation of CGO lattice by 45° with respect to STO lattice. This clearly indicates that epitaxial CGO films are realized on STO(110) basal plane due to low lattice misfit when compared to MgO(001).[9]

Figures 2(a) and 2(b) show impedance spectra measured in air at 400 °C for MgO(001)/CGO_{250nm} and MgO(001)/$STO_{10/20/50\,nm}$/CGO_{250nm} films, respectively. The spectra consist of a single non-depressed semicircle, and no electrode feature is apparent in the spectra because of their low impedance contribution. A single RC element (i.e., a resistor (R) in parallel with a capacitor (C)) is used as equivalent circuit to obtain the impedance-frequency relation at various temperatures. A single impedance arc of the polycrystalline CGO_{250nm} thin films is ascribed to the total contribution of grains and grain boundaries to the ionic conductivity. Frequency distribution shows the RC relaxation times at 400 °C for samples (Figs. 2(c) and 2(d)). Epitaxial CGO films deposited on MgO(001)/$STO_{10/20/50nm}$ at 400 °C in air relax faster (from the frequency apex values 2.5×10^{-7} s, 2.7×10^{-7} s, and 3.2×10^{-7} s, i.e., relaxation time constant $\tau = 2\pi RC$) compared to polycrystalline films (8.5×10^{-7} s) deposited

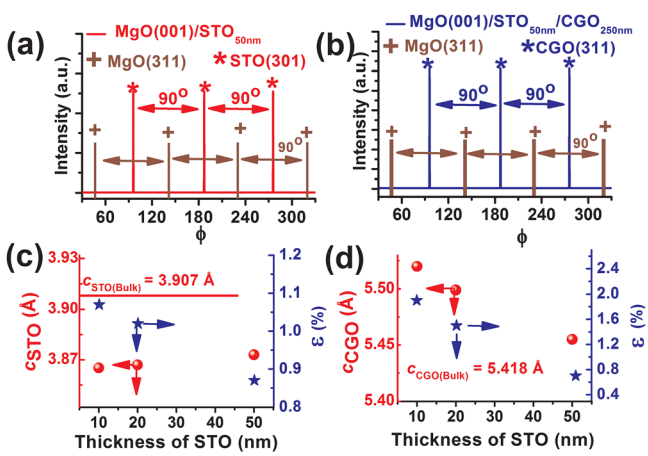

FIG. 1. (Color online) Φ—scan x-ray diffraction patterns of (a) STO_{50nm} deposited on MgO(001) and (b) CGO_{250nm} deposited on MgO(001)/STO_{50nm}. Out-of-plane lattice constants and strain in (c) STO buffer layers deposited on MgO(001) and (d) CGO_{250nm} deposited on MgO(001)/$STO_{10/20/50nm}$. Dotted lines are a guide to the eye.

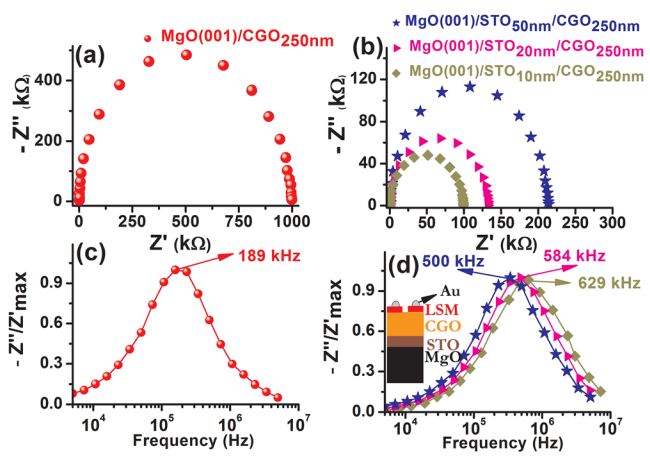

FIG. 2. (Color online) (a) and (b) are Nyquist plots whilst (c) and (d) represent frequency dependence of imaginary part of impedance measured at 400 °C for MgO(001)/CGO_{250nm} and MgO(001)/$STO_{10/20/50\,nm}$/CGO_{250nm} films, respectively. Inset in (d) shows the electrode arrangement used for *in-plane* conductivity measurements.

directly on MgO(001). The resistance measured by two probe dc method is nearly equal to the value of resistance obtained from the impedance spectrum confirming the low contribution of the electrodes polarization at the high temperatures. No thermal hysteresis was observed in polycrystalline and epitaxial CGO films deposited on MgO(001) and MgO(001)/$STO_{10/20/50\,nm}$. The capacitance values obtained for epitaxial CGO films are in the range 10^{-11}–5×10^{-12} F which are in the order of the stray capacitance (5×10^{-12} F), indicating no relevant differences between the effect of CGO_{250nm} and substrate (MgO(001)/$STO_{10/20/50\,nm}$) by impedance measurements in the *in-plane* configuration.

Epitaxial CGO_{250nm} films on STO buffer exhibit larger conductivity than the polycrystalline CGO films in the entire temperature range 400–900 °C. The conductivity curves shift upward for films with thinner STO buffer layers. MgO(001)/STO_{10nm}/CGO_{250nm} exhibits the highest conductivity (Figure 3(b)). Conductivity values for the MgO(001)/CGO_{250nm} (polycrystalline) are lower than those of epitaxial films by a factor of 3 at higher temperatures, and by more than an order of magnitude at lower temperatures. At 900 °C, CGO_{250nm} films deposited on MgO(001)/$STO_{10/20/50nm}$ exhibit two to three fold larger conductivity than in the films deposited on MgO(001) substrate. The activation energy (E_a) of MgO(001)/CGO_{250nm} was calculated to be 0.81 eV from Nyquist plots (Figure 3(a)) measurements. The calculated activation energies for MgO(001)/$STO_{10/20/50\,nm}$/CGO_{250nm} films are in the range ~0.93–0.94 eV. These activation energies correspond to the values reported for bulk doped ceria.[23] However, higher activation energy values for strained films clearly indicate an expected increase in migration and association enthalpies related to oxygen vacancy diffusion for the strained lattice when compared to the strain-free one.[14]

In polycrystalline CGO, the grain boundary acts as blocking surface and the resistance offered to oxygen ionic conduction is larger to cross the grain boundary than to through bulk/grain interior. Minimizing the grain boundary network via depositing epitaxial films leads to reduce resistance contribution from grain boundaries which results in the ionic conductivity enhancement. For coherent epitaxial growth on the three different MgO(001)/$STO_{10/20/50\,nm}$, the tuned lattice mismatch between the thin film (CGO_{250nm}) and substrate is accommodated by the strain from the STO/CGO interface throughout the thickness of the CGO film. For increasing lattice mismatch, strain is compensated by the formation of defects which aids faster oxygen diffusion.[24] As observed in the experiments, on one hand, higher strain leads to higher ionic conductivity and on the other, increased defect density (due to increase in lattice strain) leads to higher activation energy. The observed ionic conductivity enhancement in MgO(001)/$STO_{10/20/50\,nm}$/CGO_{250nm} can be thus attributed to the combination of epitaxial nature of CGO, reduction of the blocking grain boundary network, and formation of strain induced defects.

In conclusion, strained epitaxial CGO thin films are deposited on to MgO(001)/$STO_{10/20/50\,nm}$. The effects of (buffer layer induced) strain on ionic conductivity enhancement in epitaxial CGO thin films are investigated. It was found that strain in CGO thin films remarkably enhances the *in-plane* ionic conductivity in the films. This work is a striking demonstration of the significance of strain in oxygen ionic conductors.

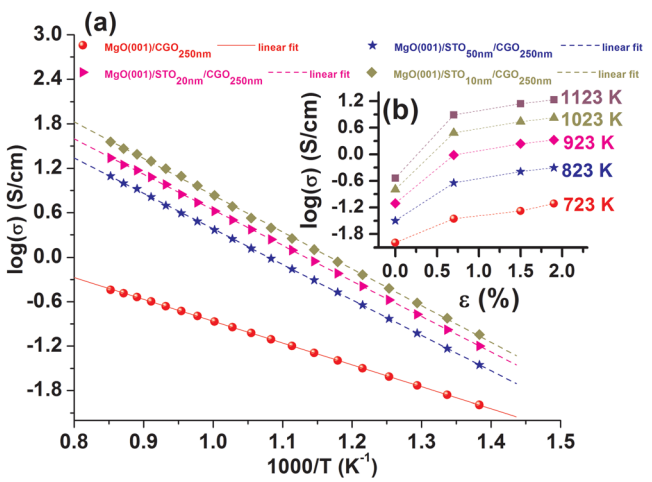

FIG. 3. (Color online) (a) Conductivity vs. temperature plots for CGO_{250nm} films deposited on MgO(001) and MgO(001)/$STO_{10/20/50nm}$ substrates. Dotted lines in figure correspond to a linear fit. (b) Conductivity vs. strain induced in CGO films measured at different temperatures. Dotted lines are a guide to the eye.

[1]B. C. H. Steele, Solid State Ionics **129**, 63 (2000).
[2]J. A. Kilner, Solid State Ionics **129**, 13 (2000).
[3]E. Gourba, A. Ringuede, M. Cassir, A. Billard, J. Paivasaari, J. Niinisto, M. Putkonen, and L. Niinisto, Ionics **9**, 15 (2003).
[4]S. J. Litzelman, J. L. Hertz, W. C. Jung, and H. L. Tuller, Fuel Cells **8**, 294 (2008).
[5]J. L. M. Rupp and L. K. Gauckler, Solid State Ionics **177**, 2513 (2006).
[6]J. B. Goodenough, Annu. Rev. Mater. Res. **33**, 91 (2003).
[7]L. Chen, C. L. Chen, X. Chen, W. Donner, S. W. Liu, Y. Lin, D. X. Huang, and A. J. Jacobson, Appl. Phys. Lett. **83**, 4737 (2003).
[8]D. X. Huang, C. L. Chen, L. Chen, and A. J. Jacobson, Appl. Phys. Lett. **84**, 708 (2004).
[9]S. Sanna, V. Esposito, D. Pergolesi, A. Orsini, A. Tebano, S. Licoccia, G. Balestrino, and E. Traversa, Adv. Funct. Mater. **19**, 1713 (2009).
[10]J. L. M. Rupp, A. Infortuna, and L. J. Gauckler, J. Am. Ceram. Soc. **90**, 1792 (2007).
[11]T. Suzuki, I. Kosacki, and H. U. Anderson, Solid State Ionics **151**, 111 (2002).
[12]I. Kosacki, T. Suzuki, V. Petrovsky, and H. U. Anderson, Solid State Ionics **136**, 1225 (2000).
[13]J. A. Kilner, Nature Mater. **7**, 838 (2008).
[14]S. Omar, E. D. Wachsman, J. L. Jones, and J. C. Nino, J. Am. Ceram. Soc. **92**, 2674 (2009).
[15]S. Omar, E. D. Wachsman, and J. C. Nino, Appl. Phys. Lett. **91**, 144106 (2007).
[16]J. A. Kilner and R. J. Brook, Solid State Ionics **6**, 237 (1982).
[17]D. J. Kim, J. Am. Ceram. Soc. **72**, 1415 (1989).
[18]I. Kosacki, C. M. Rouleau, P. F. Becher, J. Bentley, and D. H. Lowndes, Solid State Ionics **176**, 1319 (2005).
[19]S. Sanna, V. Esposito, A. Tebano, S. Licoccia, E. Traversa, and G. Balestrino, Small **6**, 1863 (2010).
[20]K. Rodrigo, S. Heiroth, M. Dobeli, N. Pryds, S. Linderoth, J. Schou, and T. Lippert, J. Optoelectron. Adv. Mater. **12**, 511 (2010).
[21]J. H. Haeni, P. Irvin, W. Chang, R. Uecker, P. Reiche, Y. L. Li, S. Choudary, W. Tian, M. E. Hawley, B. Craigo, A. K. Taganstev, X. Q. Pan, S. K. Streiffer, L. Q. Chen, S. S. Kirchoefer, J. Levy, and D. G. Scholm, Nature **430**, 758 (2004).
[22]M. Swanson, N. Tangtrakarn, M. Sunder, and P. D. Moran, Solid State Ionics **181**, 379 (2010).
[23]C. Korte, A. Peters, J. Janek, D. Hesse, and N. Zakharov, Phys. Chem. Chem. Phys. **10**, 4623 (2008).
[24]K. Otsuka, A. Kuwabara, A. Nakamura, T. Yamamoto, K. Matsunaga, and Y. Ikutata, Appl. Phys. Lett. **82**, 877 (2003).
[25]See supplementary material at http://dx.doi.org/10.1063/1.3676659 for thin film deposition details, experimental details and X-ray diffraction patterns of MgO/$STO_{10/20/50\,nm}$ and MgO/$STO_{10/20/50\,nm}$/$CGO_{250\,nm}$ thin films.